Universiteit Utrecht

Faculteit Bètawetenschappen

The electrically driven magnon Hall effect in YIG/Pt heterostructures

---

Bachelor thesis

R.L.D. Meijs

Study: Physics & Mathematics

Supervisors:

dr. R.A. Duine
Institute for Theoretical Physics

dr. S. Bender
Institute for Theoretical Physics

June 2015

Abstract

We analyze the magnon Hall effect in in a setup that utilizes an electrically driven magnon current. We give a first approximation for the transverse magnon current by looking at a setup with simplified boundary conditions and use these results to determine a simple expression for the transverse current. Furthermore we do calculations to estimate the order of magnitude of the magnon Hall conductivity in YIG/Pt heterostructures. This is done by approximating the Berry curvature for the magnetic insulator YIG. Together with the Berry curvature and the distribution function we calculate the magnon Hall conductivity. We use two different distribution functions, the Boltzmann and Bose distribution function. Using the Boltzmann distribution function we get a magnon Hall conductivity of -3.08 times the longitudinal magnon conductivity, while when using the Bose distribution we get a result of -83 times the magnon Hall conductivity. From these results we conclude that this calculation needs to be done more accurately to get meaningful result, as the Hall conductivity we find is too large to be realistic.

Contents

Chapter 1

Introduction

When an electric current goes through a conductor and a magnetic field is applied perpendicular to the electric current a transverse current is created. This effect is called the the Hall effect and was first observed by Edwin Hall in 1879 [1]. When the charge carriers move through the conductor, the combination of the magnetic field and the moving charges create a Lorentz force. The Lorentz force pushes the charge carriers sideways, thereby creating an electric potential between the two sides of the conductor.

More recently various other, similar effects have been discovered such as the quantum Hall effect and the anomalous Hall effect [2]. Also within the study of magnons, wavelike spin fluctuations in ferromagnets, a similar effect has also been discovered, the thermal magnon Hall effect [3]. This magnon Hall effect is not due to the Lorentz force, since magnons are charge-free particles, but leads to the thermal gradient in the transverse direction of the magnon current. Magnon currents are not based on moving charges, but rather on moving magnetic moments. Because there are no moving charges, magnon currents do not have dissipation due to Joule heating.

Magnon currents can be created both from a temperature gradient and a magnon potential gradient, which may be electrically induced [4]. The thermal Hall effect for magnons has already been experimentally verified by detecting the transverse magnon heat current. However , magnons currents can also be electrically driven. In this thesis we are interested in the magnon Hall effect due to an electrically driven magnon current, which is a different effect from the thermal magnon Hall effect because of the difference between how the magnon current is driven and detected. The presence of such an effect has been discussed by [5], which gives a basis to determine the size of the magnon Hall effect. In this thesis we will discuss a first approximation for the size of this transverse current for an electrically driven magnon current based on works presented in the References.

This thesis is organized as follows. In Chapter 2 we will reproduce part of the work of [4] in which we will calculate the magnon current in a longitudinal setup. In Chapter 3 we will discuss a first approximation for a transverse magnon current. To calculate this we will calculate the magnon potential and current using simplified boundary conditions. The results of this calculation we will use on the Hall geometry to make a first approximation for the magnon current in the transverse direction. In Chapter 4 we will calculate the magnon Hall conductivity for an electrically driven magnon current. We expect a magnon Hall conductivity of between 1 and 10 percent of the magnon conductivity.

Chapter 2

Longitudinal magnon transport

In this chapter we will work out the magnon current in the longitudinal setup (see Fig. 2.1). Our aim is to calculate the magnon current due to an incoming spin current, j_{s1}. The size of the incoming spin current is determined from the results of [4], for typical values see appendix. We define our magnon current in accordance with [4]:

$$\vec{j}_m(x,y) = -\frac{1}{\hbar}\begin{pmatrix} \sigma_m & \sigma_{xy} \\ -\sigma_{xy} & \sigma_m \end{pmatrix}\begin{pmatrix} \frac{\partial \mu_m}{\partial x}(x,y) \\ \frac{\partial \mu_m}{\partial y}(x,y) \end{pmatrix}, \tag{2.0.1}$$

where σ_m is the magnon conductivity in the longitudinal direction of the magnon current, σ_{xy} the magnon conductivity in the transverse direction, i.e. the magnon Hall conductivity, and μ_m the magnon chemical potential. For the purpose of this chapter we assume $\sigma_{xy} = 0$ and $\frac{\partial \mu_m}{\partial y}(x,y) = 0$, since we only look at the longitudinal magnon current and assume that there is no transverse effect.

2.1 Setup

Fig. 2.1 shows the geometry of the ferromagnetic insulator (FI) we will look at. We only look at the 2 dimensional system because the system is independent on the z-coordinate, so we will not take into account the height of the geometry. The size in the y-direction is assumed to be much larger than the magnon diffusion length and therefore we don't take into account the edges at $y = 0$ and $y = L_y$. Furthermore we do not take into account the interface current between the normal metal (NM) and FI layers, since we assume that there is no spin-potential in the NM layers.

2.2 Equations

From[4] we get the following equation to describe this system:

$$\zeta\left(\frac{3}{2}\right)\nabla^2\mu_m + \frac{5k_B}{2}\zeta\left(\frac{5}{2}\right)\nabla^2 T_m = \frac{1}{l_m^2}\left[\zeta\left(\frac{3}{2}\right)\mu_m + \frac{5k_B}{2}\zeta\left(\frac{5}{2}\right)(T_m - T_{ph})\right],$$

where l_m is the magnon diffusion length, ζ is the Riemann-Zeta function, k_B the Boltzmann constant, T_m the magnon temperature and T_{ph} the phonon temperature.Since we assume that there is no temperature gradient, this leads to

$$\mu_m(x) = l_m^2 \frac{d\mu_m(x)}{dx}. \tag{2.2.1}$$

For this equation we have the general solution $\mu_m(x) = a_1 e^{x/l_m} + a_2 e^{-x/l_m}$, where a_1 and a_2 are constants of integration. But if $L_x \gg l_m$ we have to neglect the a_1 term and the solution reduces to:

$$\mu_m(x) = a_2 e^{-x/l_m} \tag{2.2.2}$$

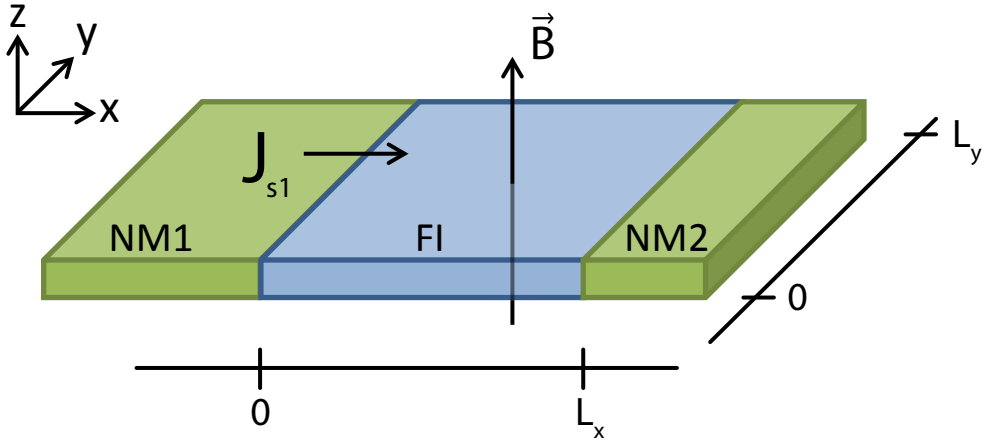

Figure 2.1 – The longitudinal setup. The green blocks are normal metals (NM) and the blue block is a ferromagnetic insulator (FI). The FI layer has a length of L_x in the x-direction and L_y in the y-direction. $\vec{B}$ is the magnetization. The length of the NM layers in the x-direction is not important for these calculations. We apply a constant spincurrent j_{s1} into the FI layer, for used data see appendix A.

2.3 Boundary conditions

Now that we have all the equations to describe the magnon current we need the boundary condition to calculate the integration constants.

At the interface between NM1 and FI we have that, because of conservation of angular momentum, the spin current is equal to the magnon current. Thus we have the following boundary condition:

$$j_{s1} = j_m(0).$$

This we can work out by using Eq. 2.0.1, which results in:

$$j_{s1} = -\frac{\sigma_m}{\hbar}\frac{d\mu_m}{dx}(0). \tag{2.3.1}$$

2.4 Result

Now using the boundary condition 2.3.1 together with 2.2.2 we can solve this system, which gives

$$\mu_m(x) = \frac{j_{s1} l_m \hbar}{\sigma_m} e^{-\frac{x}{l_m}}.$$

This gives the following solution for the magnon current:

$$j_m(x) = j_{s1} e^{-\frac{x}{l_m}}. \tag{2.4.1}$$

In Fig. 2.2 we have plotted the magnon current. From this plot we can see that the magnon current decreases when the distance to the NM1 layer increases. The outgoing magnon current into the NM2 layer is exponentially suppressed as a function of L_x, with a characteristic length l_m.

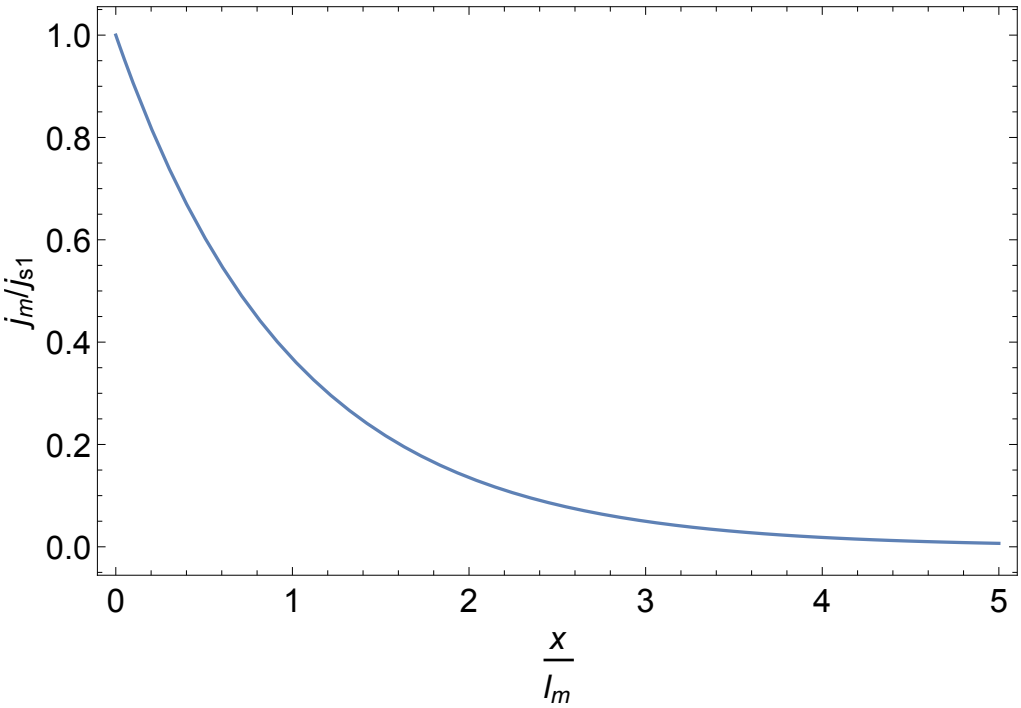

Figure 2.2 – The longitudinal magnon current as a function of x over the magnon diffusion length in the longitudinal setup in the FI layer. For used data see appendix A.

Chapter 3

Hall geometry

In this chapter we will make a first approximation for a transverse, electrically driven magnon current. To make a first approximation of the transverse magnon current we will look at the hard wall setup (see Fig. 3.1). This means that we assume that no spin current leaves the system in the transverse direction. This is a reasonable approximation as we expect the magnon Hall conductivity to be small compared tot the longitudinal conductivity. With this geometry we want to calculate the longitudinal magnon current, which we will use to make a first estimate of the magnon current in the transverse direction. Compared to the setup used in Chapter 2 there is no outgoing magnon current.

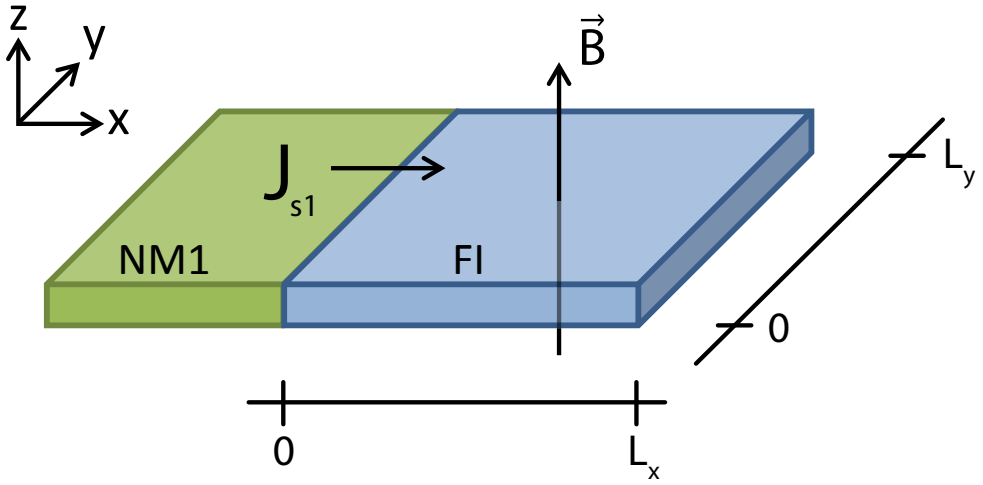

Figure 3.1 – The hard wall setup; the green block is a NM layer and the blue block is a FI layer. The FI layer has a length of L_x in the x-direction and L_y in the y-direction. $\vec{B}$ is the magnetization. The length of the NM1 layer in the x-direction is not important for these calculations. Here we apply a constant spin current, j_{s1}, from the NM layer. For used data see appendix A.

This setup we will call the hard wall setup. From the left we apply a spin current which will create a magnon potential in the FI layer. There is only a NM layer on one side, all the other sides have hard walls, which cannot conduct. We assume that there is no spin potential in the NM layer and therefore we also neglect the interface current.

3.1 Equations and boundary conditions

The magnon current is again only driven by the magnon potential, thus to calculate the magnon current in the FI layer we need to solve the following differential equation:

$$\mu_m(x,y) = l_m^2 \nabla^2 \mu_m(x,y).$$

This system has the following boundary conditions:

$$\begin{aligned} \frac{\partial}{\partial x}\mu_m(0,y) &= \frac{-j_{s1}\hbar}{\sigma_m} \\ \frac{\partial}{\partial x}\mu_m(L_x,y) &= 0. \end{aligned} \tag{3.1.1}$$

The first boundary condition is due to the conservation of angular momentum at the first interface (similar as with the longitudinal setup). The second boundary condition comes from the fact that there is no spin current at the right side of the device due to the hard walls. Lastly we assume that there is no gradient of the magnon potential in the y-direction because of the symmetry of the system.

3.2 Solution and results

Now with these boundary conditions we can solve our system, which gives the following solution:

$$\mu_m(x) = \frac{j_{s1} l_m \hbar e^{-\frac{x}{l_m}} \left(e^{\frac{2L_x}{l}} + e^{\frac{2x}{l_m}} \right)}{\sigma_m \left(e^{\frac{2L_x}{l_m}} - 1 \right)}. \tag{3.2.1}$$

Using Eq. 2.0.1 we can calculate the magnon current (see Eq. 3.2.2). We plotted the magnon current in both directions in Figs. 3.2 and 3.3. It is clear that the magnon current in both directions decreases when we get further away from the NM layer. In the x-direction the result is very similar to the result from Chapter 2. This can be understood by looking at what happens when L_x goes to infinity. In this limit we get the same result as in Chapter 2. From Figs. 3.2 and 3.3 we can also see that $|\frac{j_{my}}{j_{mx}}| = \frac{\sigma_{xy}}{\sigma_m}$. The result for both components of the magnon spin current is:

$$\vec{j}_m = \frac{j_{s1} e^{-\frac{x}{l_m}} \left(e^{\frac{2L_x}{l_m}} - e^{\frac{2x}{l_m}} \right)}{e^{\frac{2L_x}{l_m}} - 1} \begin{pmatrix} 1 \\ -\frac{\sigma_{xy}}{\sigma_m} \end{pmatrix}. \tag{3.2.2}$$

In Appendix B we give the derivation of a system of equations to get a better solution for the magnon potential.

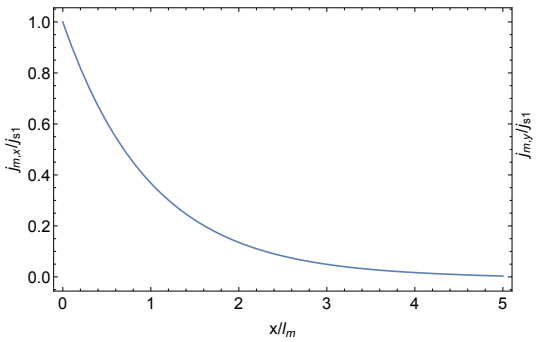

Figure 3.2 – The magnon current in the x-direction of the hard wall setup (see Figure: 3.1) as function of the distance with respect to the magnon diffusion length l_m for the hard wall geometry. For L_x we used 10^{-4} m, see Appendix A for the other parameters.

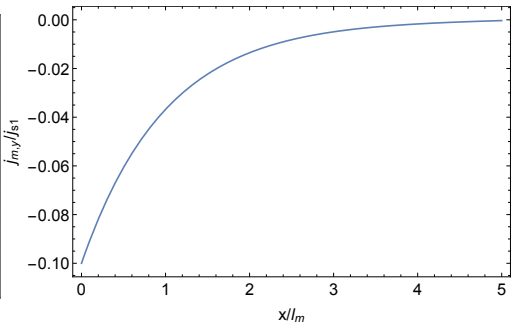

Figure 3.3 – The magnon current in the y direction of the hard wall setup (see Figure: 3.1) as function of the distance with respect to the magnon diffusion length l_m for the hard wall geometry. Where we used $L_x = 10^{-4}$ m and $\sigma_{xy} = \frac{\sigma_m}{10}$, see Appendix A for the other parameters.

3.3 Magnon current in y direction

Now that we have found the magnon current we will calculate a first approximation of the magnon current in the y-direction. Therefore we will look at the Hall geometry (see Fig. 3.4). In this geometry we use the solution from the hard wall setup to find the outgoing magnon current at the interface between FI and NM2.

In this setup we place a second NM at the top of the device. This NM2 layer is of length Δ and is placed at (L, L_y) . The outgoing magnon current can be calculated by integrating the magnon current over the surface, which leads to the following expression:

$$I_{out} = \int_{L-\frac{\Delta}{2}}^{L+\frac{\Delta}{2}} dx j_{my} = \frac{\sigma_{xy}}{\sigma_m} 2 j_{s1} l_m \sinh\left(\frac{\Delta}{2l_m}\right) \operatorname{csch}\left(\frac{L_x}{l_m}\right) \sinh\left(\frac{L - L_x}{l_m}\right). \tag{3.3.1}$$

To discuss the result of Eq. 3.3.1, we will use the following:

$$\lim_{x\to\infty} \operatorname{csch}(x)\sinh(x) = 1$$

$$\lim_{x\to 0} \operatorname{csch}(x)\sinh(x) = 1.$$

This means that when $L, L_x \gg l_m$ and $L \sim L_x$ that $I_{out} \approx 0$. While when $L, L_x \ll l_m$, then $I_{out} \approx \frac{\sigma_{xy}}{\sigma_m} 2 j_{s1} l_m \sinh\left(\frac{\Delta}{2l_m}\right)$. From Fig. 3.5 it is clear that when the NM2 layer is placed further away from the NM1 layer, the outgoing current decreases rapidly. If we compare this with Fig. 3.3 we see that this happens at the same distance, which is a logical result since the outgoing current is proportional to the magnon current in the y-direction. Another result that can be deduced from Eq. 3.3.1 is that the outgoing current becomes zero when $L_x \approx 0$. This is also as expected since when there is no FI layer, there should not be any magnon current in the y-direction.

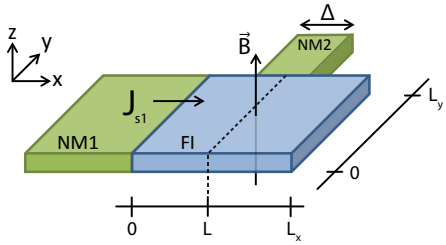

Figure 3.4 – The Hall geometry, this is the same geometry as 3.1 with the addition of a second NM2 layer of size Δ at the top of the device with the middle positioned at (L, L_y). See Appendix A for the size of j_{s1}.

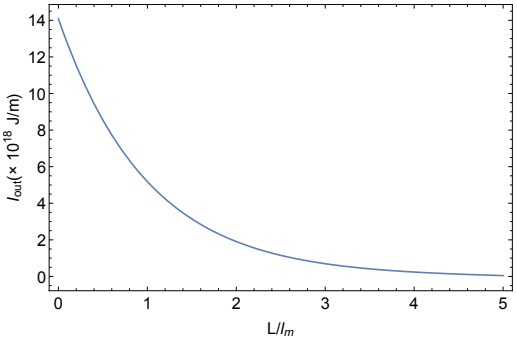

Figure 3.5 – The I_{out} as a function of the placement of the NM2 layer L with respect to the magnon diffusion length l_m. Where we used $L_x = 10^{-4}$m, $\sigma_{xy} = \frac{\sigma_m}{10}$ and $\Delta = l_m$, for the other parameters used see (Appendix A)

Chapter 4

Determining the magnon Hall conductivity

In this chapter we will use the results from [5] to calculate a first approximation of the magnon Hall conductivity, σ_{xy}.

4.1 Relating σ_{xy} to L_{11}

We start with the linear response of the magnon current, from [5]:

$$\mathbf{j} = L_{11}[-\nabla U - \nabla\mu] + L_{12}\left[T\nabla\left(\frac{1}{T}\right)\right],$$

which is related to the heat current $\mathbf{j}_Q = \mathbf{j}_E - \mu\mathbf{j}$; where j_E is the energy current and L_{11}, L_{12} and U are defined as in [5]. Since we only look at a magnon current driven by the magnon potential, we assume that there is no temperature gradient. Thus this gives the following expression for the magnon current:

$$\mathbf{j} = -L_{11}\nabla\mu. \tag{4.1.1}$$

Now we want to relate this equation to the definition of the magnon current we use Eq. 2.0.1. This can be done by checking the units of both definitions. One has [5]:

$$L_{11} = -\frac{1}{\hbar V}\sum_{n,\mathbf{k}}\Omega_{n,z}(\mathbf{k})\rho(\epsilon_n), \tag{4.1.2}$$

where V is the thickness of the sample, $\Omega_{n,z}$ the Berry curvature in momentum space and ρ the distribution function. From [5] we get that $[V] = \mathrm{m}^2$, $[\Omega_{n,z}(\mathbf{k})] = 1/\mathrm{m}^2$, ρ is dimensionless and $[\hbar] = \mathrm{Js}$. This leads to

$$[L_{11}] = 1/\mathrm{Js}.$$

Note that $\mathbf{j}_Q$ used in [5] is the two dimensional heat current density, thus $[\mathbf{j}_Q] = \frac{1}{\mathrm{m}^2}\mathrm{J}\frac{\mathrm{m}}{\mathrm{s}} = \frac{\mathrm{J}}{\mathrm{m\ s}}$.

We can compare this to the unit of σ_m, for which we use [4] and [6] and we obtain

$$[\sigma_m] = \frac{\mathrm{Js}}{\mathrm{m}}.$$

The difference in units of σ_m and L_{11} comes from the fact that [4] uses $[\mathbf{j}_m] = \frac{\mathrm{J}}{\mathrm{m}^2}$, which is the three dimensional current density. Thus to calculate σ_{xy} from L_{11} we therefore use following formula:

$$\sigma_{xy} = \frac{L_{11}\hbar^2}{L}, \tag{4.1.3}$$

where L is the thickness of the sample.

4.2 Equations

Now that we have found Eq. 4.1.3, we can start to calculate L_{11}. We begin by defining the different elements from Eq. 4.1.2. $\Omega_{n,z}(\mathbf{k})$ is the Berry curvature in momentum space, $\rho(\epsilon_n)$ is the Bose distribution function of the n-th band and V is the area of the sample. The summation of n is over all the bands and the summation over $\mathbf{k}$ is over the momenta.

For the Berry curvature we will use the following approximation, which is found in [5]:

$$\Omega_{n,z}(\mathbf{k})/L^2 \simeq \begin{cases} \left(\frac{1}{4}\frac{M_0}{H_0}\right)^2 & \text{if } n = 0; \\ \frac{1}{2}\left(\frac{1}{n\pi}\right)^4 \left(\frac{M_0}{H_0}\right)(kL)^2 & \text{if } n > 0, \end{cases} \tag{4.2.1}$$

where M_0 is the saturation magnetization and H_0 the internal static magnetic field. The Bose distribution function is defined as $\rho(\epsilon_n) = (e^{\beta(\epsilon_n - \mu)} - 1)^{-1}$ with $\epsilon_n = \hbar\omega_n$ and we assume that we are in equilibrium thus $\mu = 0$. In order to calculate the integrals we will both use the Bose distribution as well as the Boltzmann distribution function $(e^{-\beta\epsilon_n})$ to approximate the Bose distribution. We use this approximation to simplify the problem and get easier calculations. For ω_n we use the same approximation as found in [5], where $\omega_n = \omega_H + \Delta\omega_n$ with:

$$\Delta\omega_n = \begin{cases} \frac{1}{4}\omega_M kL & \text{if } n = 0 \\ \frac{\omega_M}{2}\left(\frac{kL}{n\pi}\right)^2 & \text{if } n > 0, \end{cases} \tag{4.2.2}$$

where $\omega_M = \gamma M_0$ and $\omega_H = \gamma H_0$ and γ the gyromagnetic ratio.

4.3 Calculating L_{11} with the Boltzmann distribution

We can rewrite L_{11} in terms of the integral over $\mathbf{k}$, which gives us:

$$\begin{aligned} L_{11} = & -\tfrac{1}{\hbar}\textstyle\sum_n \int \frac{d\mathbf{k}}{(2\pi)^2}\Omega_{n,z}(\mathbf{k})\rho(\epsilon_n) \\ = & -\tfrac{1}{\hbar}\textstyle\sum_n \int d\theta \int dk\ k \frac{1}{(2\pi)^2}\Omega_{n,z}(k)\rho(\epsilon_n) \\ = & -\tfrac{1}{\hbar}\textstyle\sum_n \int 2\pi \frac{1}{(2\pi)^2} dk\ k\ \Omega_{n,z}(k)\rho(\epsilon_n). \end{aligned}$$

The area element cancels because of the integration and in the intermediate step we went to polar-coordinates.

4.3.1 Boundaries of integration

In order to compute the integrals inside the sum, we need to determine the integration bounds because the integral diverges. This we do by using that the total number of magnon modes is equal to the number of lattice sites so that $\int_0^\Lambda \frac{d\mathbf{k}}{(2\pi)^2} = s$, where s is the spin-density. So now we can determine the cut-off Λ:

$$\int_0^\Lambda \frac{d\mathbf{k}}{(2\pi)^2} = \int_0^{2\pi} d\theta \int_0^\Lambda dk \frac{k}{(2\pi)^2} = \int_0^\Lambda dk \frac{k}{2\pi} = \frac{1}{4\pi}\Lambda^2 = s,$$
$$\Rightarrow \Lambda = \sqrt{4\pi s}$$

Now that we know the boundary of integration, we can compute the different integrals.

4.3.2 Calculating the integrals

For $n = 0$ we have:

$$\int_0^\Lambda dk \frac{1}{2\pi} k\ \Omega_{0,z}\rho(\epsilon_0) = \int_0^\Lambda dk \frac{1}{2\pi}\ k\ \left(\frac{1}{4}\frac{LM_0}{H_0}\right)^2 \frac{1}{e^{\beta\hbar(w_H+\frac{1}{4}\omega_M kL)}}$$
$$= -\frac{M_0^2\left(\sqrt{\pi}\beta L\sqrt{s}w_M\hbar - 2e^{\frac{1}{2}\sqrt{\pi}\beta L\sqrt{s}w_M\hbar}+2\right)e^{-\frac{1}{2}\beta\hbar\left(\sqrt{\pi}L\sqrt{s}w_M+2w_H\right)}}{4\pi\beta^2 H_0^2 w_M^2\hbar^2},$$

and, for $n > 0$, we have

$$\int_0^\Lambda dk \frac{1}{2\pi} k\ \Omega_{n,z}\rho(\epsilon_0) = \int_0^\Lambda dk \frac{1}{2\pi} k \frac{1}{2}\left(\frac{1}{n\pi}\right)^4\left(\frac{M_0}{H_0}\right)(kL)^2 e^{-\beta\hbar(w_H+\frac{\omega_M}{2}\left(\frac{kL}{n\pi}\right)^2)}$$
$$= \frac{M_0^2\left(\pi n^2\left(e^{\frac{2\beta L^2 s w_M\hbar}{\pi n^2}}-1\right)-2\beta L^2 s w_M\hbar\right)e^{\beta\hbar\left(-\left(\frac{2L^2 s w_M}{\pi n^2}+w_H\right)\right)}}{2\pi^2\beta^2 H_0^2 n^2 w_M^2\hbar^2}.$$

Combining these results we calculate L_{11}. We are interested in the rate of convergence, which we can see in Fig. 4.1a. From this figure we can see that L_{11} converges rapidly when the number of terms added increases. From this we conclude that if we compute the sum from $n = 0$ to $n = 100$ we have a good approximation of the actual value of L_{11}.

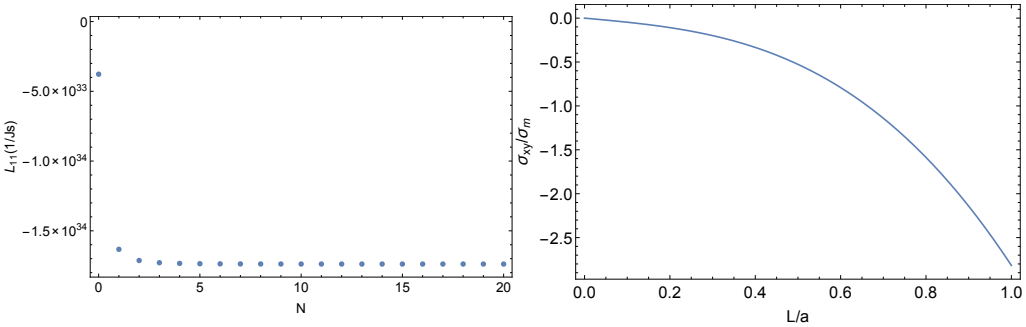

(a) The convergence rate of L_{11} as a function of the size of the sum. We used $L = 10^{-9}$ m and $\beta\hbar\omega_H = 0.01$, for the other parameters see Appendix A.

(b) The size of the Hall angle $\frac{\sigma_{xy}}{\sigma_m}$ as a function of the thickness of the FI layer L with respect to the lattice vector. We used $\beta\hbar\omega_H = 0.01$, for the other parameters see Appendix A.

Figure 4.1

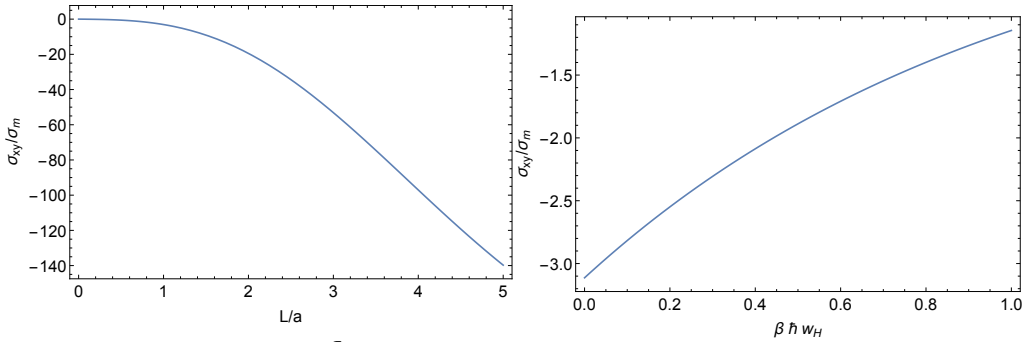

(a) The size of the Hall angle $\frac{\sigma_{xy}}{\sigma_m}$ as a function of the thickness of the FI layer L with respect to the lattice vector. We used $\beta\hbar\omega_H = 0.01$, for the other parameters see Appendix A.

(b) The size of the Hall angle $\frac{\sigma_{xy}}{\sigma_m}$ as a function of the product $\beta\hbar\omega_H$. We used $L = 10^{-9}$ m, for the other parameters see Appendix A.

Figure 4.2

From Fig. 4.2a we see that when L is more then twice the size of the lattice vector the Hall angle $\frac{\sigma_{xy}}{\sigma_m}$ increases rapidly. This is a surprising result as we excepted that the transverse current should be smaller then longitudinal current. It is clear that our approximation does not work when we increase the thickness of our sample. When reviewing [5] this can be explained by the fact that the authors work with a two dimensional system. What is even more unexpected is that the Hall angle is only smaller then 1 when $L/a < 0.6$ and $\beta\hbar\omega_H = 0.01$. We expected to see a small Hall angle, of the order of 0.1. We can also see that as $\beta\hbar\omega_H$ is increased the Hall angle goes to zero. For $L = a$ and $\beta\hbar\omega_H = 0.01$ the Hall angle is -3.08.

4.4 Calculating L_{11} with the Bose distribution

In this section we will calculate L_{11} while using the Bose-Einstein distribution function. The calculations are very similar as in section 4.3. We can use the same integration boundary and rewrite the integral in polar coordinates. We will now evaluate the integrals:

$$\begin{aligned}\int_0^\Lambda dk \tfrac{1}{2\pi} k\ \Omega_{0,z}\rho(\epsilon_0) &= \int_0^\Lambda dk \tfrac{1}{2\pi}\ k\ \left(\tfrac{1}{4}\tfrac{LM_0}{H_0}\right)^2 \tfrac{1}{e^{\beta\hbar(w_H+\frac{1}{4}\omega_M kL)}-1} \\ &= -\tfrac{M_0^2}{16\pi\beta^2 H_0^2\omega_M^2\hbar^2}\Bigg[\pi\beta^2L^2s\omega_M^2\hbar^2 - 8\mathrm{Li}_2\left(e^{\omega_H\beta\hbar+\frac{1}{2}L\omega_M\beta\sqrt{\pi}\sqrt{s}\hbar}\right) \\ &\quad -4\sqrt{\pi}\beta L\sqrt{s}\omega_M\hbar\log\left(1-e^{\frac{1}{2}\sqrt{\pi}\beta L\sqrt{s}\omega_M\hbar+\beta\omega_H\hbar}\right)+8\mathrm{Li}_2\left(e^{\omega_H\beta\hbar}\right)\Bigg],\end{aligned}$$

and, for $n > 0$,

$$\begin{aligned}\int_0^\Lambda dk \tfrac{1}{2\pi} k\ \Omega_{n,z}\rho(\epsilon_0) &= \int_0^\Lambda dk \tfrac{1}{2\pi} k \tfrac{1}{2}\left(\tfrac{1}{n\pi}\right)^4\left(\tfrac{M_0}{H_0}\right)(kL)^2\tfrac{1}{e^{\beta\hbar(w_H+\frac{\omega_M}{2}\left(\frac{kL}{n\pi}\right)^2)}-1} \\ &= -\tfrac{M_0^2}{2\pi^3\beta^2H_0^2n^4\omega_M^2\hbar^2}\Bigg[2\beta L^2s\omega_M\hbar\ \times \\ &\quad \left(\beta L^2s\omega_M\hbar-\pi n^2\log\left(1-e^{\beta\hbar\left(\frac{2L^2s\omega_M}{\pi n^2}+\omega_H\right)}\right)\right) \\ &\quad -\pi^2n^4\mathrm{Li}_2\left(e^{\left(\frac{2s\omega_ML^2}{n^2\pi}+\omega_H\right)\beta\hbar}\right)+\pi^2n^4\mathrm{Li}_2\left(e^{\omega_H\beta\hbar}\right)\Bigg].\end{aligned}$$

In these expressions $\mathrm{Li}_2(x) = \sum_{k=1}^{\infty}\frac{x^k}{k^2}$, which is the polylogarithmic function. With the found results we can calculate L_{11}. In Fig. 4.3a we can see the convergence rate of L_{11}. It's clear that the first 5 terms are the most important terms, so we have decided to evaluate the sum up to $n = 100$. With this amount of terms we believe that there is a good balance between calculation speed and accuracy.

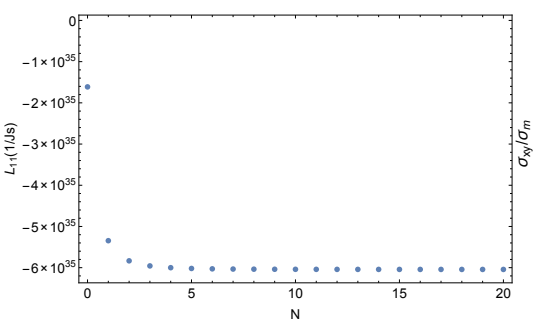

(a) The convergence rate of L_{11} as a function of the size of the sum. We used $L = 10^{-9}$ m and $\beta\hbar\omega_H = 0.01$, for the other parameters see Appendix A.

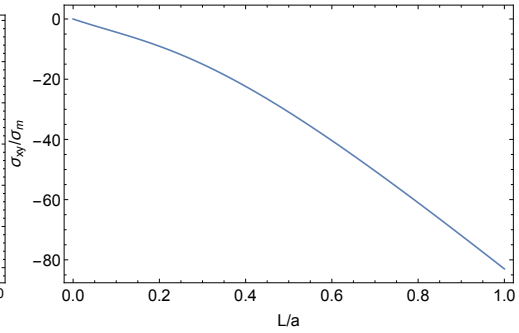

(b) The size of the Hall angle $\frac{\sigma_{xy}}{\sigma_m}$ as a function of the thickness of the FI layer L with respect to the lattice vector. We used $\beta\hbar\omega_H = 0.01$, for the other parameters see Appendix A.

Figure 4.3

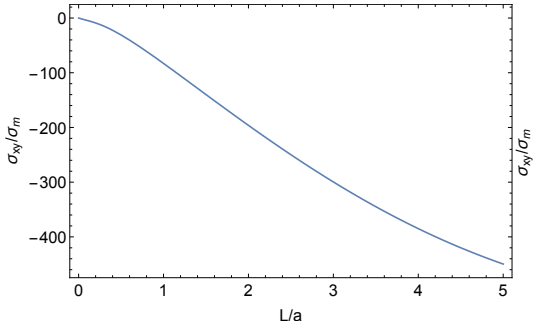

(a) The size of the Hall angle $\frac{\sigma_{xy}}{\sigma_m}$ as a function of the thickness of the FI layer L with respect to the lattice vector. We used $\beta\hbar\omega_H = 0.01$, for the other parameters see Appendix A.

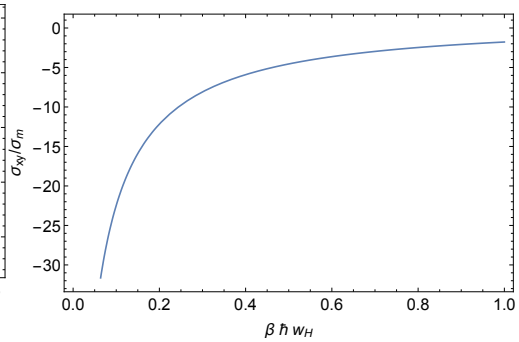

(b) The size of the Hall angle $\frac{\sigma_{xy}}{\sigma_m}$ as a function of the product $\beta\hbar\omega_H$. We used $L = 10^{-9}$ m, for the other parameters see Appendix A.

Figure 4.4

The results of the Hall angle with using the Bose distribution show the same behavior as with the Boltzmann distribution. With this calculation the Hall angle is larger for all values of L/a and $\beta\hbar\omega_H$ compared to the calculation with using the Boltzmann distribution. Likely this is because the low-energy states contribute most, and are given a higher weight in the Bose distribution. Furthermore the Hall angle increases and becomes much larger than expected as the thickness increases. The Hall angle also converges to zero, which means there will be no magnon current in the transverse direction when the strength of the external field is increased. For $L = a$ and $\beta\hbar\omega_H = 0.01$ the Hall angle is -83.

Chapter 5

Conclusion

In this thesis we studied the transverse magnon current due to a chemical magnon potential. We started from the result of [4] to calculate the magnon potential. We reproduced part of this work as a starting point to calculate the transverse magnon current. After this we looked at a first approximation to calculate the transverse magnon current, where we calculated the magnon potential in the hard wall geometry and then placed an extra NM layer on top of the device. From this we could calculate a magnon current in the y-direction. To calculate this we used σ_{xy} as a transverse magnon conductivity. Lastly we made an estimate of the magnitude of σ_{xy} based on [5], which we did with both the Boltzmann and the Bose distribution.

From this first calculation of σ_{xy} we can conclude our used approximations are not accurate enough to calculate a physically sensible magnon Hall conductivity . The results that we got from this calculation were much larger than we expected. Our initial thoughts were to find a magnon Hall conductivity between 1 and 10 percent of the magnon conductivity σ_m. In our calculations the magnon hall conductivity is $-3.08\sigma_m$ when using the Boltzmann distribution function and $-83\sigma_m$ when using the Bose distribution function. We don't think this is a physical result and therefore more research is needed.

The calculations of σ_{xy} can be made better by also taking into account the z-direction. This has to be done in different parts of the calculations. First, the integration over k-space should be made three dimensional. Second, the Berry curvature needs to be calculated in the three dimensional momentum space. Another assumption is that $k \sim 0$, from which the approximations of ω_n was made. Since our boundary of integration is of order $10^{10}\mathrm{m}^{-1}$, this assumption is not valid over the whole surface of integration. Furthermore the Berry curvature is calculated using these approximations, but for calculating the magnon Hall conductivity the whole Berry curvature has to be taken into account and not just an approximation for $k \sim 0$. Lastly, solving the drift diffusion equations more accurately is important to find a more accurate prediction for the experimentally detected signal.

Appendix A

Data used

See [4] and [6].

j_{s1}	$-1.4379 \times 10^{-11}\mathrm{J/m^2}$
l_m	9.4×10^{-6} m
σ_m	$1.08611 \times 10^{-25}\mathrm{Js/m}$
$g_{\uparrow\downarrow}$	$5 \times 10^{18}\mathrm{m^{-2}}$
S	10
Λ_m	6.24231×10^{8} m
$\frac{M_0}{H_0}$	1
$\beta\hbar\omega_m$	0.01
s	6.529×10^{18}
a	12.376×10^{-10} m

Appendix B

Higher order approximation Hall geometry

Here we derive a system of equations to approximate the magnon current in the hall geometry to a higher order. In this approximation we assume that $\sigma_{xy} \ll \sigma_m$ and define $\eta = \frac{\sigma_{xy}}{\sigma_m}$. With this we can write the magnon chemical potential as:

$$\mu_m(x,y) = \sum_{i=0} \eta^i \mu_i(x,y). \tag{B.0.1}$$

Again we assume that there is no temperature gradient, which gives us the following equation to solve:

$$\mu_m(x,y) = l_m^2 \vec{\nabla}^2 \mu_m(x,y). \tag{B.0.2}$$

For this system we have the following boundary conditions:

$$\begin{aligned} \tfrac{\vec{j}_m(0,y)}{\sigma_m} &= -\tfrac{1}{\hbar} \begin{pmatrix} \frac{\partial \mu}{\partial x}(0,y) + \eta \frac{\partial \mu}{\partial y}(0,y) \\ \frac{\partial \mu}{\partial y}(0,y) - \eta \frac{\partial \mu}{\partial x}(0,y) \end{pmatrix} = \begin{pmatrix} \frac{j_{s1}}{\sigma_m} \\ 0 \end{pmatrix} \\ \tfrac{\vec{j}_m(L_x,y)}{\sigma_m} &= -\tfrac{1}{\hbar} \begin{pmatrix} \frac{\partial \mu}{\partial x}(L_x,y) + \eta \frac{\partial \mu}{\partial y}(L_x,y) \\ \frac{\partial \mu}{\partial y}(L_x,y) - \eta \frac{\partial \mu}{\partial x}(L_x,y) \end{pmatrix} = 0 \end{aligned}, \tag{B.0.3}$$

where we have divided by σ_m in order to get η in our boundary conditions.

Now we will look at the different orders of μ_i by substituting B.0.1 into B.0.3. This gives us the following relations:

$$\begin{aligned} &\tfrac{\partial}{\partial x} \textstyle\sum_{i=0} \eta^i \mu_i(x,y) + \eta \tfrac{\partial}{\partial y} \sum_{i=0} \eta^i \mu_i(x,y) = \tfrac{j_{s1}}{\sigma_m} \\ &\tfrac{\partial}{\partial y} \textstyle\sum_{i=0} \eta^i \mu_i(x,y) - \eta \tfrac{\partial}{\partial x} \sum_{i=0} \eta^i \mu_i(x,y) = 0 \end{aligned}. \tag{B.0.4}$$

Now we have to take into account the zero-order term. For $\mu_0(x,y)$ the following holds:

$$\begin{aligned} \mu_0(x,y) &= l_m^2 \vec{\nabla}^2 \mu_0(x,y) \\ \vec{\nabla}\mu_0(0,y) &= -\tfrac{\hbar}{\sigma_m} j_{s1} \\ \vec{\nabla}\mu_0(L_x,y) &= 0. \end{aligned} \tag{B.0.5}$$

However the zero-order term gives the magnon chemical potential when there is no magnon Hall effect, thus $\frac{\partial \mu_0}{\partial y} = 0$. This leads to the same system as in Chapter 3, which we can solve exactly (see Eq. 3.2.2).

Now we can combine B.0.4 and B.0.5 to get the following system of equations:

$$
\begin{array}{lcl|rcl}
\mu_0(x,y) & = & l_m^2 \frac{\partial^2}{\partial^2 x}\mu_0(x,y) & \mu_i(x,y) & = & l_m^2 \vec{\nabla}^2 \mu_i(x,y) \\
\frac{\partial}{\partial x}\mu_0(0,y) & = & -\frac{\hbar}{\sigma_m} j_{s1} & \frac{\partial}{\partial x}\mu_i(0,y) & = & -\frac{\partial}{\partial y}\mu_{i-1}(0,y) \\
\frac{\partial}{\partial x}\mu_0(L_x,y) & = & 0 & \frac{\partial}{\partial y}\mu_i(0,y) & = & \frac{\partial}{\partial x}\mu_{i-1}(0,y) \\
\frac{\partial}{\partial x}\mu_i(L_x,y) & = & -\frac{\partial}{\partial y}\mu_{i-1}(L_x,y) & \frac{\partial}{\partial y}\mu_i(L_x,y) & = & \frac{\partial}{\partial x}\mu_{i-1}(0,y)
\end{array}
\tag{B.0.6}
$$

With these equations the magnon potential can be solved up to a certain order. Solving these systems is left for further research.

Bibliography

[1] Edwin Hall. On a new action of the magnet on electric currents. *American Journal of Mathematics*, 2(3):287–292, Sept 1879.

[2] Di Xiao, Ming-Che Chang, and Qian Niu. Berry phase effects on electronic properties. *Rev. Mod. Phys.*, 82:1959–2007, Jul 2010.

[3] Y. Onose, T. Ideue1, H. Katsura, Y. Shiomi, N. Nagaosa, and Y. Tokura. Observation of the magnon hall effect. *Science*, 329(5989):297–299, Jul 2010.

[4] Kevin Peters. Magnon-mediated current drag in the semiclassical regime. Bachelor thesis, Utrecht University, 6 2015.

[5] Ryo Matsumoto and Shuichi Murakami. Rotational motion of magnons and the thermal hall effect. *Phys. Rev. B*, 84:184406, Nov 2011.

[6] Ludo J Cornelissen, Kevin JH Peters, Rembert A Duine, Gerrit EW Bauer, and Bart J van Wees. Magnon spin transport driven by the magnon chemical potential in a magnetic insulator. *arXiv preprint arXiv:1604.03706*, 2016.